

Article

Multi-Temporal InSAR Structural Damage Assessment: The London Crossrail Case Study

Pietro Milillo ^{1,*}, Giorgia Giardina ² , Matthew J. DeJong ³, Daniele Perissin ⁴ and Giovanni Milillo ⁵ 

¹ Jet Propulsion Laboratory, 4800 Oak Grove Drive, Pasadena, CA 91109, USA

² Department of Architecture and Civil Engineering, University of Bath, Claverton Down, Bath BA2 7AY, UK; g.giardina@bath.ac.uk

³ Department of Engineering, University of Cambridge, Trumpington St., Cambridge CB2 1PZ, UK; mjd97@cam.ac.uk

⁴ Lyles School of Civil Engineering, Purdue University, West Lafayette, IN 47907, USA; perissin@purdue.edu

⁵ Agenzia Spaziale Italiana, Contrada Terlecchia, Matera, MT 75100, Italy; giovanni.milillo@asi.it

* Correspondence: pietro.milillo@jpl.nasa.gov

Received: 18 December 2017; Accepted: 7 February 2018; Published: 13 February 2018

Abstract: Spaceborne multi-temporal interferometric synthetic aperture radar (MT-InSAR) is a monitoring technique capable of extracting line of sight (LOS) cumulative surface displacement measurements with millimeter accuracy. Several improvements in the techniques and datasets quality led to more effective, near real time assessment and response, and a greater ability of constraining dynamically changing physical processes. Using examples of the COSMO-SkyMed (CSK) system, we present a methodology that bridges the gaps between MT-InSAR and the relative stiffness method for tunnel-induced subsidence damage assessment. The results allow quantification of the effect of the building on the settlement profile. As expected the greenfield deformation assessment tends to provide a conservative estimate in the majority of cases (~71% of the analyzed buildings), overestimating tensile strains up to 50%. With this work we show how these two techniques in the field of remote sensing and structural engineering can be synergistically used to complement and replace the traditional ground based analysis by providing an extended coverage and a temporally dense set of data.

Keywords: multi-temporal InSAR; InSAR; tunneling; subsidence; relative stiffness method; structural engineering; damage assessment; soil-structure interaction

1. Introduction

MT-InSAR is a well-established monitoring technique capable of extracting time-series of LOS surface displacements. It was born around the end of the 1990s in order to overcome traditional InSAR limitations such as atmospheric artifacts, and temporal and geometrical decorrelation when long ERS interferometric stacks of data started being available [1,2]. Since then several improvements have been made on both the algorithms and the quality of the data. In particular, the availability of high resolution and short repeat time satellite constellations lead to more effective near real-time disaster monitoring, assessment response and greater ability to constrain dynamically changing physical processes [3,4]. Although many studies have been carried out using InSAR in the field of structural monitoring looking at urban areas [5–7], bridges [8,9], railways [10,11], tunneling [12–15], and dams [16–19], state of the art scientific literature sees only few papers coupling MT-InSAR and structural modeling as a building damage assessment tool [6,20–22].

Several procedures have been proposed in civil engineering to predict the structural damage caused by underground excavations to adjacent structures (e.g., [23,24]). One of the key factors for an

accurate damage assessment is the quantification of the soil-structure interaction, which influences the settlement profile originated by the excavation [25–28]. Attempts have been made to include this effect in simplified procedures for the damage assessment of large scale urban projects, by connecting the building-induced variation of the settlement profile with the relative stiffness between the structure and the soil [29–32]. Structural engineering literature compared the outcome of these methods with experimental [26,33] and numerical [27,29–31] data, but their potentials and limitations need to be assessed against large datasets of field measurements to further validate their practical application [34].

In this paper we propose a new integrated damage assessment methodology that aims to bridge the gaps between InSAR time-series analysis and the relative stiffness method for the assessment of tunneling-induced structural damage [32]. Our dataset includes 72 images acquired from April 2011 to December 2015 combined to produce time-series of cumulative deformation over the city of London (UK), where the Crossrail twin tunnels were excavated starting in 2012 [35]. We compare our InSAR dataset to a dense set of ground based measurements acquired over 14 buildings, showing how the MT-InSAR time-series product can overcome the lack of ground based monitoring of building displacements and thus facilitate the application of damage assessment procedures which take the soil-structure interaction mechanism into account [34].

The paper is organized as follows: Section 2 describes the data and the area of interest together with the Crossrail project. Section 3 describes briefly the MT-InSAR methodologies and the relative stiffness method. Section 4 presents and discusses the results and the modeling. Conclusions are provided in Section 5.

2. Dataset and Area of Interest

Our dataset includes 72 CSK images acquired from April 2011 to December 2015, combined to produce time-series of cumulative deformation and ground based measurements of 14 buildings affected by tunneling induced subsidence. The ground data was obtained from the Underground Construction Information Management System (UCIMS), a web-based geotechnical data management system designed for the project [36].

CSK is a constellation of 4 low Earth orbit satellites carrying an X-band SAR antenna (3.1 cm wavelength) enabling a better (3 m) resolution and sampling rate (up to 176.25 MHz) of ground displacements than longer wavelength systems (e.g., 6 cm for C-band, 24 cm for L-band). Each satellite has a repeat cycle of 16 days, but shorter repeats may be achieved using the constellation. Here, we used data acquired from the CSK background mission covering all the largest cities worldwide with a population bigger than one hundred thousand inhabitants with an average sampling rate of 16 days. The SAR image dataset is formed by a stack of CSK STRIPMAP-HIMAGE covering a 40×40 km swath, at 3 m resolution in both azimuth (along track) and range (cross track) directions. Polarization of the electromagnetic waves is HH (horizontal transmit and receive). The incidence angle is ~ 29 degrees across the swath.

We analyzed a sub-area of the entire frame in single-look complex (SLC) format of $5 \text{ km} \times 5 \text{ km}$ in the azimuth and range directions, respectively (Figure 1). The analyzed area covers the central route section of the Crossrail project, which is currently the largest underground excavation project in Europe and involves the boring of 21 km of twin tunnel of 6.2 m diameter and up to 40 m deep, and the construction of 10 new stations under central London.

The local geology of the region of London under consideration consists of layers (from top to bottom) of Terrace Deposits, London clay, the Lambeth Group (gravels, sands, silt, and clay), Thanet sands, and Chalk. Tunneling was primarily through the London clay and Lambeth Group layers, resulting in settlements with the typical characteristics of tunneling in soft ground. In the region two aquifers are present, with piezometric surface at approximately zero Ordnance Datum (OD) and between -40 m and -50 m OD, respectively [37].

The tunneling was executed by soft-ground pressure-balance tunnel-boring machines between May 2012 and May 2015. Compensation grouting was adopted in several locations along the tunnel

route and near the stations to minimize ground settlements. The 14 selected buildings are located directly above, or in close proximity to, the tunnel track (Figure 1), and therefore were potentially at risk of being damaged by the tunnel-induced settlement [37].

To verify the accuracy of the MT-InSAR measurements, the satellite-based ground displacements of one transect transverse to the tunnel track were compared with the displacements measured by Precise Levelling Points (PLP). The PLPs were installed on the ground prior to the beginning of the excavation and could measure the difference in elevation between two or more points with high orders of accuracy (0.3–0.9 mm). In this work, we used precise levelling measurements acquired with daily frequency between May 2012 and August 2014, and therefore covering the passage of the tunnel boring machine in the area of interest. The analysis of the data confirmed the typical Gaussian shape of the settlement trough along the tunnel, combined with larger settlements near to the station excavations.

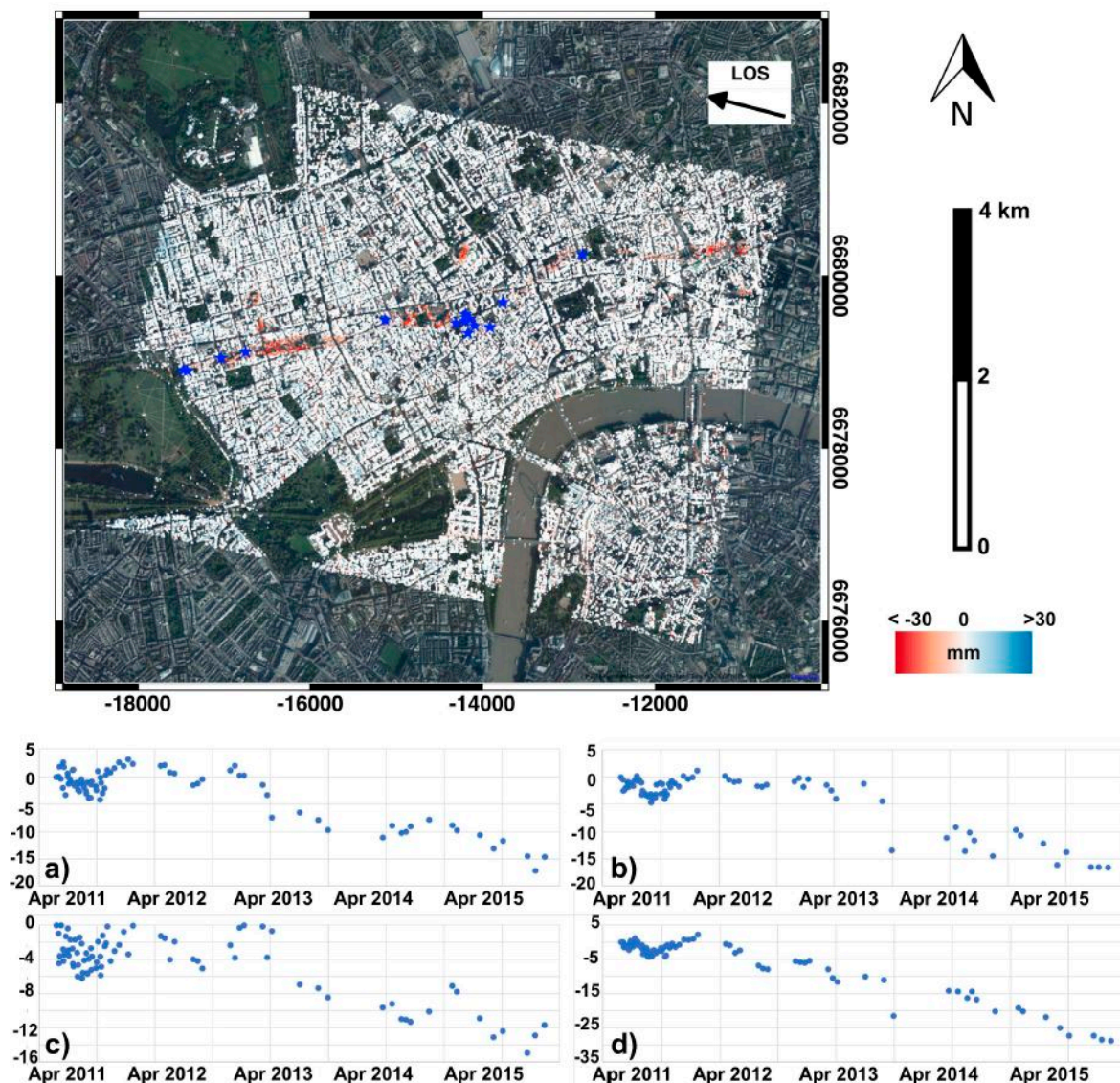


Figure 1. Cumulative displacement map over London spanning April 2011–December 2015. Negative values indicate subsidence. Blue stars indicate the locations of the analysed buildings. (a–d) represent the locations of the non-linear time series analysis, which are shown beneath the satellite image (in mm).

3. Methodology

3.1. MT-InSAR

Synthetic aperture radar multi temporal interferometry (MT-InSAR) is a well established technique for ground deformation monitoring characterized by millimetric accuracy [1,18]. MT-InSAR combines sets of SAR images acquired in interferometric mode in order to obtain time-series of deformation for points on the ground maintaining stable scattering properties in time [1,38]. MT-InSAR measurements provide coverage of ground deformation at high resolution and spatial scales not reasonably accessible with in situ measurements such as leveling and GPS.

A variety of software tools are available for implementing multi-image InSAR techniques. In this work we make use of SARPROZ [39] and adopt a non-linear single master multi-temporal time series analysis approach [38]. For further details on the technique we refer the reader to [1,38,39].

3.2. Building Damage Assessment Relative Stiffness Method

Common procedures for the assessment of settlement-induced structural damage start with the evaluation of the tensile strains caused by the greenfield settlement profile when applied to the base of a linear elastic beam model of the building [24]. The soil greenfield displacements are defined as tunneling-induced ground displacements in absence of buildings. They are usually calculated analytically or numerically neglecting the influence of the structure weight and stiffness, while considering the type of soil, the tunnel depth and diameter, and the volume of ground lost during the excavation [40–42]. The settlement profile depicted in Figure 2 is typical of tunneling in soft ground.

The severity of the applied ground distortion is quantified by the deflection ratio Δ/L (Figure 2). For any given two points on the soil surface, Δ/L is the ratio of the relative deflection Δ and their horizontal distance L . Δ is defined as the maximum vertical distance from the settlement profile between the two points and a straight line connecting them. The distance L typically corresponds to the length of the building either in the sagging (L_{sag}) or hogging (L_{hog}) part of the greenfield settlement profile (Figure 2).

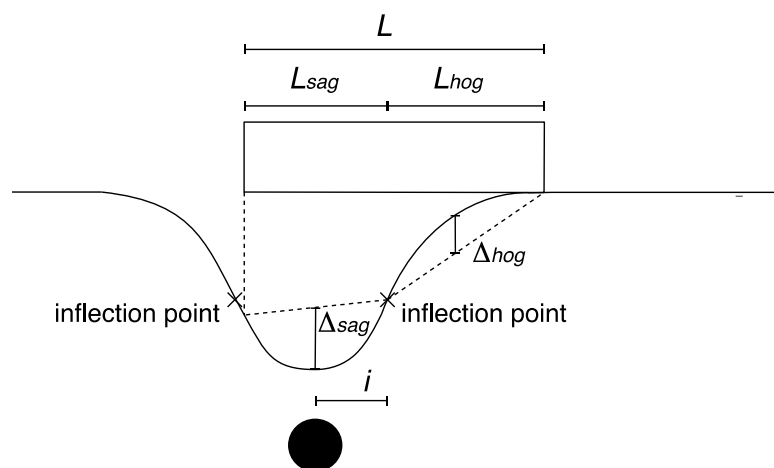


Figure 2. Typical shape of a tunneling-induced settlement trough. The inflection point separates the sagging (sag) from the hogging (hog) zone. The relative deflection and building length for each zone are indicated with Δ and L .

The greenfield beam strains are then approximated using the calculated deflection ratio, and are then compared to pre-defined limiting strain values which relate to a certain level of expected damage [24]. Each building damage level is described in terms of approximate crack widths, as summarized in Table 1.

The building weight and stiffness typically has the effect of widening the soil settlement profile, thus reducing its curvature. For this reason, the deflection ratio calculated in greenfield conditions is generally bigger than the actual one resulting from the soil-structure interaction effect. This simplified method therefore provides conservative damage predictions [43].

Table 1. Damage classification of building, based on limiting tensile strain levels and expected crack width [24,44].

Category of Damage	Damage Class	Approximate Crack Width	Limiting Tensile Strain Levels (%)
Aesthetic damage	Negligible	Up to 0.1 mm	0–0.05
	Very slight	Up to 1 mm	0.05–0.075
	Slight	Up to 5 mm	0.075–0.15
Functional damage, affecting serviceability	Moderate	5 to 15 mm or a number of cracks > 3 mm	0.15–0.3
	Severe	15 to 25 mm, but also depends on number of cracks	>0.3
Structural damage, affecting stability	Very severe	Usually > 25 mm, but depends on number of cracks	>0.3

A more accurate assessment method takes into consideration the fact that the soil-structure interaction modifies the shape and magnitude of the settlement profile, thus affecting the final damage classification and decision-making process. Modification factors [29,31,32] have been defined to account for the difference between greenfield distortions (Δ_{gr}/L_{gr}), and actual distortions (Δ/L), and therefore to update the tensile strains to more realistic values. In this paper we consider the modification factor for the deflection ratio, which is defined as the ratio between the actual deflection ratio of the building and the greenfield deflection ratio of the soil surface [29]:

$$MF = \frac{(\Delta/L)}{(\Delta_{gr}/L_{gr})} \quad (1)$$

If a building spans over the inflection point (Figure 2), the modification factors are calculated separately for the sagging and hogging part of the trough. Note that buildings affect not only the relative deflection Δ but also the location of the inflection point, and therefore the length L_{sag} and L_{hog} of the building partition in the sagging and hogging zones, respectively. If the actual Δ/L is not known a-priori, e.g., for damage prediction, the modification factors can be obtained by using design curves based on building and soil characteristics [29,31,32]. The derived $\Delta/L = MF (\Delta_{gr}/L_{gr})$ are then used to calculate the tensile strain of the linear elastic beam of the building according to Timoshenko beam theory [24,45].

In this paper we investigate how MT-InSAR measurements can be used, in combination with the relative stiffness method, to rapidly evaluate potential tunneling-induced building damage by providing information on the actual soil-structure mechanism which would be otherwise inaccessible. In particular our procedure and validation can be summarized in the following steps: (a) analytical calculation of the greenfield displacement fields (i.e., zero height) for the Crossrail project, (b) comparison and validation of the analytical greenfield settlement profile with persistent scattering (PS) points located on the ground, (c) calculation of the PS based deflection ratio for the selected buildings and modification factor calculation as in Equation (1), (d) derivation of the building strains and their comparison with the greenfield strains.

4. Results and Discussion

Approximately 228,000 persistent scatterers have been identified over a 25 km² area in London (Figure 1) for an overall density of 9000 PS/km². Figure 3 shows how the typical transverse settlement profile caused by the tunneling-induced loss of ground can be recognized from the cumulative displacement field. Time-series analysis of points located over different areas reveal subsidence varying from 2 cm to 3.5 cm, providing a precise assessment tool able to monitor the current progress

of excavation works (Figure 1a–d). The PS density enabled by the high-resolution X-band CSK constellation in urban areas allows to capture subsidence profiles of sections transverse to the tunnel axis (Figures 3 and 4). The comparison between InSAR PS and precise levelling points (PLP) on the ground (Figure 3) indicates a reasonable match between the two datasets (5.5 mm standard deviation for PS with temporal coherence higher than 0.8 and 2.5 mm for PS with temporal coherence higher than 0.9). The graph in Figures 3 and 4 includes the Gaussian curve typically used to model tunneling-induced greenfield displacements [40].

The soil-structure interaction effect is measured by the difference between the greenfield and building displacements (Figure 4), which are responsible for the actual damage. Figure 4 also shows the displacements of the PS located on top of the building.

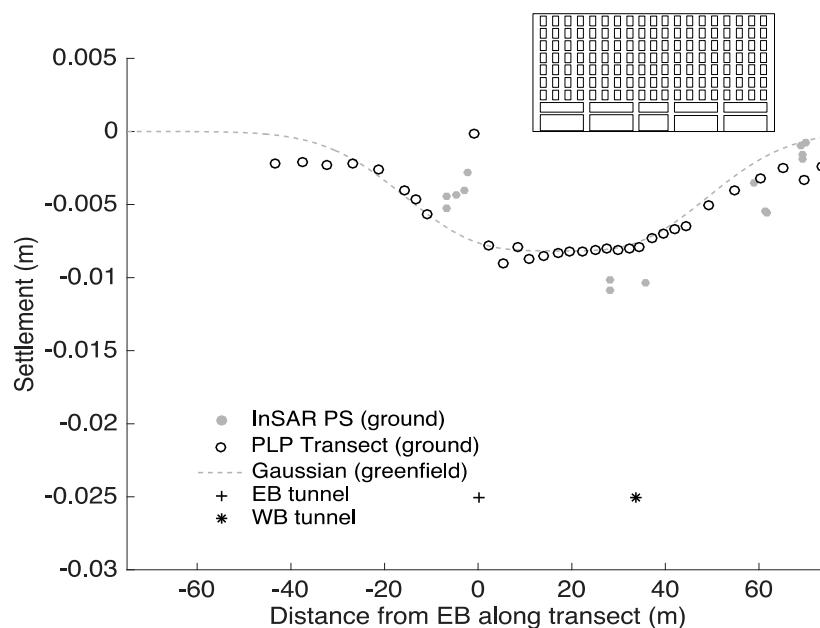


Figure 3. Example of ground- and MT-InSAR-based displacements at the ground level (adjacent to the building). The EB and WB tunnel markers indicate the centerline of the Eastbound and Westbound tunnels respectively.

To assess the building damage within the framework of the relative stiffness method we implemented the following procedure: first we validated the greenfield model with the PS tunnel cross section shown in Figure 3. Because relatively small horizontal strains are transferred to buildings [24,25,28], for each building we selected PS cross sections localized on the roof and projected them onto the vertical. We interpolated the PS points using a modified Gaussian model [46,47] (Figure 4) and calculate the Δ/L values (see Figure 2). We derived the sagging and hogging modification factors by dividing these values by the corresponding (Δ_{gr}/L_{gr}) , obtained through fitting the PLP data with an appropriate Gaussian curve, as illustrated in Figure 3. Figure 5 shows the modification factors resulting from the analysis of 14 sample buildings. The modification factors were obtained for the sagging and hogging part of each structure settlement trough, according to Equation 1. Due to their relative high stiffness with respect to the soil stiffness, the buildings tend to reduce the curvature of the greenfield settlement profile, leading to modification factors smaller than 1 for the majority of the analyzed cases. The modification factors can then be used to directly approximate the building strain which is then used to classify the building damage.

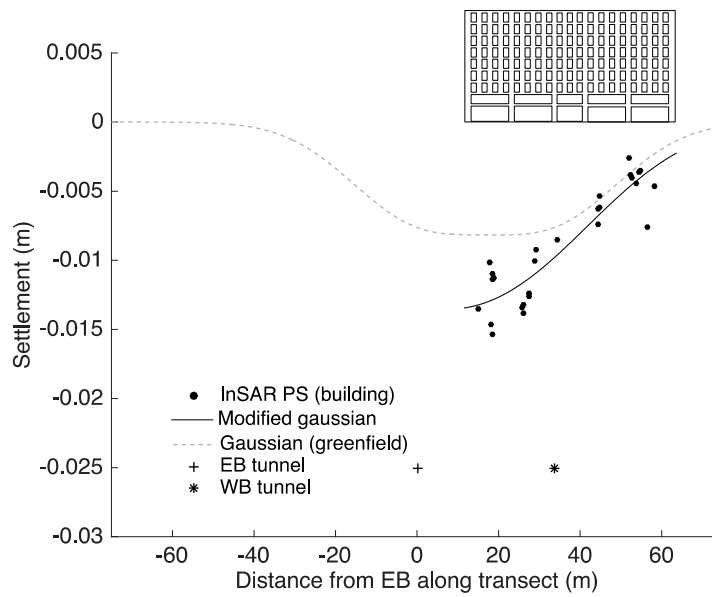


Figure 4. Example of MT-InSAR-based displacements at the top of the building.

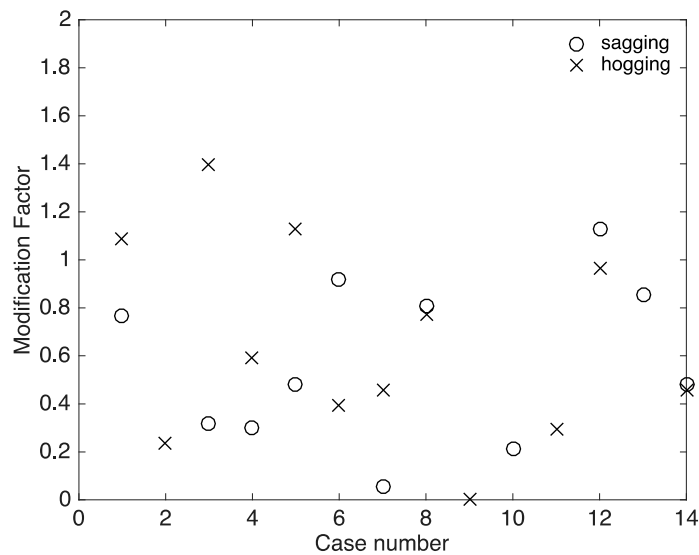


Figure 5. MT-InSAR-based building modification factors.

Figure 6 shows the building tensile strains based on the InSAR monitoring data in relation to their corresponding greenfield values. About 71% of the analyzed buildings fall below the 1:1 line, indicating the expected conservative tendency of the greenfield-based assessment. The smaller the values, the larger the flattening effect of the structure on the greenfield profile. Figure 7 shows a schematic representation of the proposed method.

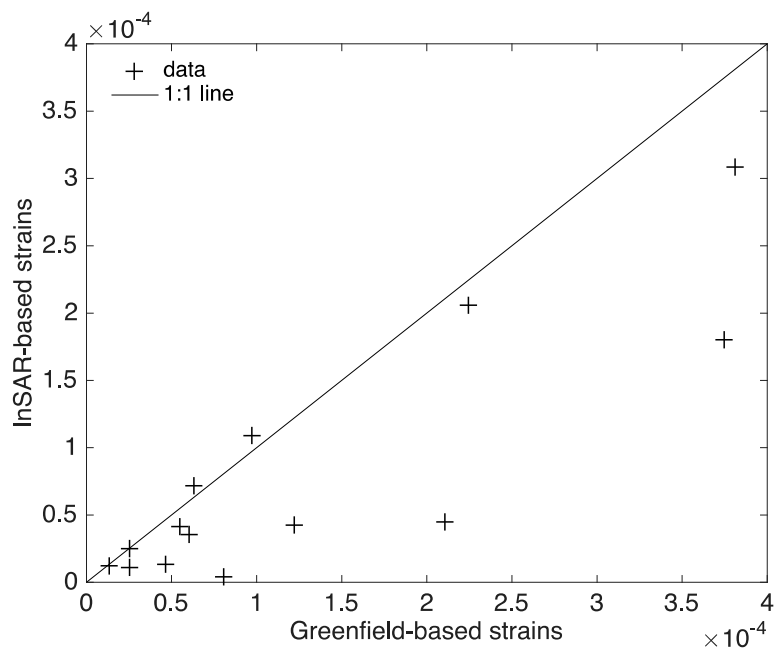


Figure 6. Greenfield-based vs. InSAR-based building strains.

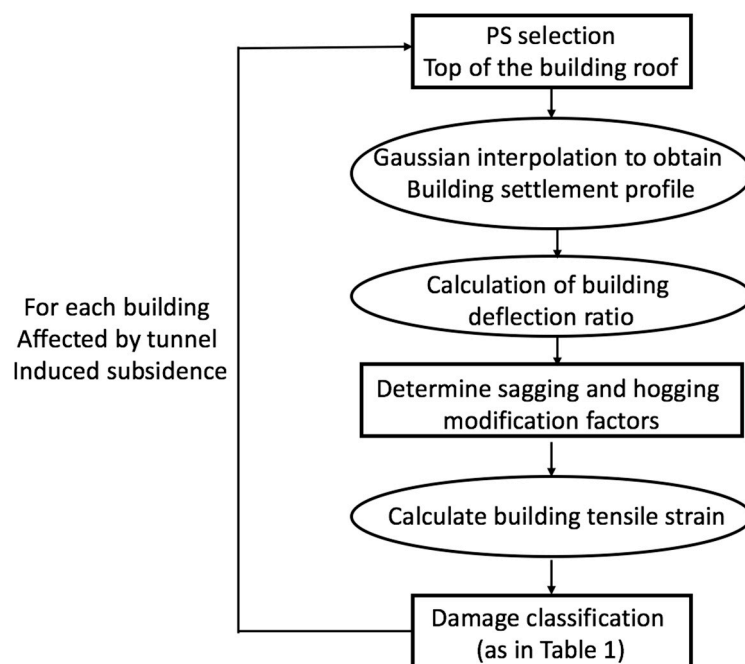


Figure 7. Schematic representation of the proposed method of the T-InSAR/relative stiffness method.

5. Conclusions

In this paper we applied two techniques in the field of remote sensing and structural engineering to assess building damage due to tunneling. Several procedures have been proposed in literature for predicting structural damage induced by underground excavations. The quantification of the soil-structure interaction effect is one of the key factors for an accurate damage assessment. Attempts to include this effect in large scale urban damage assessment procedures have been performed connecting the building-induced variation of the settlement profile with the relative stiffness between the structure and the soil [29–32]. However, the lack of assessment and validation against large datasets of field

measurements has highlighted the difficulty of assessing their potential and consequently their practical application [34].

The proposed approach demonstrates how the use of MT-InSAR time-series analysis can be coupled to the relative stiffness method in order to calculate building modification factors. These modification factors can then be used to assess building damage caused by tunneling-induced subsidence. We have demonstrated the feasibility of this approach jointly exploiting two differential techniques, bridging the gaps between remote-sensing space-borne observations and structural engineering analysis. We validated our PS cumulative displacement fields using ground based leveling measurements and found a standard deviation of 2.5 mm for PS with temporal coherence higher than 0.9. The results show the difference between building and greenfield movements (Figure 6), allowing quantification of the effect of the building on the settlement profile. As expected the greenfield deformation assessment tends to provide a conservative estimate in the majority of cases (10 of the 14 buildings), overestimating tensile strains up to 50%. Future research will point toward the creation of an automatic system capable of generating tunneling induced damage maps including PS time-series analysis, building and soil characteristics.

Acknowledgments: Original COSMO-SkyMed product ASI Agenzia Spaziale Italiana (2011–2016). We wish to thank Deborah Lazarus and David Ashworth for providing the leveling data included in Figure 3. We wish to thank Sang-Ho Yun for hosting Giorgia Giardina at NASA-JPL while writing this paper. This research was carried out at the Jet Propulsion Laboratory, California Institute of Technology, under a contract with the National Aeronautics and Space Administration.

Author Contributions: Pietro Milillo and Giovanni Milillo Processed the SAR data. Daniele Perissin Supervised the SAR data processing. Giorgia Giardina and Matthew J. DeJong worked on the structural engineering calculations. Pietro Milillo wrote the paper and interpreted the results supported by Giorgia Giardina, Giovanni Milillo, Daniele Perissin and Matthew J. DeJong.

Conflicts of Interest: The authors declare no conflict of interest.

References

1. Ferretti, A.; Prati, C.; Rocca, F. Permanent scatterers in SAR interferometry. *IEEE Trans. Geosci. Remote Sens.* **2001**, *39*, 8–20. [[CrossRef](#)]
2. Berardino, P.; Fornaro, G.; Lanari, R.; Sansosti, E. A new algorithm for surface deformation monitoring based on small baseline differential SAR interferograms. *IEEE Trans. Geosci. Remote Sens.* **2002**, *40*, 2375–2383. [[CrossRef](#)]
3. Milillo, P.; Riel, B.; Minchew, B.; Yun, S.H.; Simons, M.; Lundgren, P. On the synergistic use of SAR constellations' data exploitation for earth science and natural hazard response. *IEEE J. Sel. Top. Appl. Earth Obs. Remote Sens.* **2016**, *9*, 1095–1100. [[CrossRef](#)]
4. Yun, S.-H.; Hudnut, K.; Owen, S.; Webb, F.; Simons, M.; Sacco, P.; Gurrola, E.; Manipon, G.; Liang, C.; Eric Fielding, E.; et al. Rapid Damage Mapping for the 2015 Mw 7.8 Gorkha Earthquake Using Synthetic Aperture Radar Data from COSMO–SkyMed and ALOS-2 Satellites. *Seismol. Res. Lett.* **2015**, *86*, 1549–1556. [[CrossRef](#)]
5. Di Martire, D.; Paci, M.; Confuorto, P.; Costabile, S.; Guastaferro, F.; Verta, A.; Calcaterra, D. A nation-wide system for landslide mapping and risk management in Italy: The second Not-ordinary Plan of Environmental Remote Sensing. *Int. J. Appl. Earth Obs. Geoinf.* **2017**, *63*, 143–157. [[CrossRef](#)]
6. Cerchiello, V.; Tessari, G.; Velterop, E.; Riccard, P.; Defilippi, M.; Pasquali, P. Risk of building damage by modeling interferometric time series. In Proceedings of the 2016 IEEE International Geoscience and Remote Sensing Symposium (IGARSS), Beijing, China, 10–15 July 2016; pp. 7334–7337.
7. Bonì, R.; Cigna, F.; Bricker, S.; Meisina, C.; McCormack, H. Characterisation of hydraulic head changes and aquifer properties in the London Basin using Persistent Scatterer Interferometry ground motion data. *J. Hydrol.* **2016**, *540*, 835–849. [[CrossRef](#)]
8. Fornaro, G.; Reale, D.; Verde, S. Bridge thermal dilation monitoring with millimeter sensitivity via multidimensional SAR imaging. *IEEE Geosci. Remote Sens. Lett.* **2013**, *10*, 677–681. [[CrossRef](#)]
9. Lazecky, M.; Perissin, D.; Bakon, M.; de Sousa, J.M.; Hlavacova, I.; Real, N. Potential of satellite InSAR techniques for monitoring of bridge deformations. In Proceedings of the Urban Remote Sensing Event (JURSE), Lausanne, Switzerland, 30 March–1 April 2015; pp. 1–4.

10. Luo, Q.; Zhou, G.; Perissin, D. Monitoring of Subsidence along Jingjin Inter-City Railway with High-Resolution TerraSAR-X MT-InSAR Analysis. *Remote Sens.* **2017**, *9*, 717. [[CrossRef](#)]
11. Chang, L.; Dollevoet, R.P.; Hanssen, R.F. Nationwide Railway Monitoring Using Satellite SAR Interferometry. *IEEE J. Sel. Top. Appl. Earth Obs. Remote Sens.* **2017**, *10*, 596–604. [[CrossRef](#)]
12. Strozzi, T.; Delaloye, R.; Poffet, D.; Hansmann, J.; Loew, S. Surface subsidence and uplift above a headrace tunnel in metamorphic basement rocks of the Swiss Alps as detected by satellite SAR interferometry. *Remote Sens. Environ.* **2011**, *115*, 1353–1360. [[CrossRef](#)]
13. Perissin, D.; Wang, Z.; Lin, H. Shanghai subway tunnels and highways monitoring through Cosmo-SkyMed Persistent Scatterers. *ISPRS J. Photogramm. Remote Sens.* **2012**, *73*, 58–67. [[CrossRef](#)]
14. Robles, J.G.; Black, M.; Gomar, B.S. *Correlation Study between In-Situ Auscultation and Satellite Interferometry for the Assessment of Nonlinear Ground Motion on Crossrail London*; Crossrail Learning Legacy Report; ICE Publishing: London, UK, 2016.
15. Martí, J.G.; Nevard, S.; Sanchez, J. *The Use of InSAR (Interferometric Synthetic Aperture Radar) to Complement Control of Construction and Protect Third Party Assets*; Crossrail Learning Legacy Report; Crossrail Ltd.: London, UK, 2017.
16. Milillo, P.; Perissin, D.; Salzer, J.T.; Lundgren, P.; Lacava, G.; Milillo, G.; Serio, C. Monitoring dam structural health from space: Insights from novel InSAR techniques and multi-parametric modeling applied to the Pertusillo dam Basilicata, Italy. *Int. J. Appl. Earth Obs. Geoinf.* **2016**, *52*, 221–229. [[CrossRef](#)]
17. Milillo, P.; Bürgmann, R.; Lundgren, P.; Salzer, J.; Perissin, D.; Fielding, E.; Biondi, F.; Milillo, G. Space geodetic monitoring of engineered structures: The ongoing destabilization of the Mosul dam, Iraq. *Sci. Rep.* **2016**, *6*, 37408. [[CrossRef](#)] [[PubMed](#)]
18. Di Martire, D.; Iglesias, R.; Monells, D.; Centolanza, G.; Sica, S.; Ramondini, M.; Pagano, L.; Mallorquí, J.J.; Calcaterra, D. Comparison between differential SAR interferometry and ground measurements data in the displacement monitoring of the earth-dam of Conza della Campania (Italy). *Remote Sens. Environ.* **2014**, *148*, 58–69. [[CrossRef](#)]
19. Emadali, L.; Motagh, M.; Haghighi, M.H. Characterizing post-construction settlement of the Masjed-Soleyman embankment dam, Southwest Iran, using TerraSAR-X SpotLight radar imagery. *Eng. Struct.* **2017**, *143*, 261–273. [[CrossRef](#)]
20. Tapete, D.; Cigna, F. Satellite-based preventive diagnosis: Use of Persistent Scatterer Interferometry on cultural heritage sites in Italy. In Proceedings of the Remote Sensing and Photogrammetry Society Conference, London, UK, 12–14 September 2012.
21. Arangio, S.; Calò, F.; Di Mauro, M.; Bonano, M.; Marsella, M.; Manunta, M. An application of the SBAS-DInSAR technique for the assessment of structural damage in the city of Rome. *Struct. Infrastruct. Eng.* **2014**, *10*, 1469–1483. [[CrossRef](#)]
22. Bonano, M.; Calò, F.; Manunta, M.; Marsella, M.; Scifoni, S.; Sonnessa, A.; Tagliaferro, V. Ground Settlement Assessment in Urban Areas through SBAS-DInSAR Measurements: The Case Study of Roma (Italy). In *Engineering Geology for Society and Territory-Volume 5*; Springer: Cham, Switzerland, 2015; pp. 985–988.
23. Mair, R.J.; Taylor, R.N.; Burland, J.B. Prediction of ground movements and assessment of risk of building damage due to bored tunneling. In *Geotechnical Aspects of Underground Construction in Soft Ground: Proceedings of the International Symposium*; Mair, R.J., Taylor, R.N., Eds.; CRC Press: Balkema, Rotterdam, 1996; pp. 713–718.
24. Burland, J.B.; Mair, R.J.; Standing, R.N. Ground performance and building response due to tunneling. In *Conference on Advances in Geotechnical Engineering*; Jardine, R.J., Potts, D.M., Higgins, K.G., Eds.; Institution of Civil Engineers: London, UK, 2004; Volume 1, pp. 291–342.
25. Viggiani, G.; Standing, J. *Building Response to Tunnelling: Case Studies from Construction of the Jubilee Line Extension*; Ciria and Thomas Telford: London, UK, 2001; Volume 2, pp. 401–432.
26. Farrell, R.P. *Tunnelling in Sands and the Response of Buildings*. Ph.D. Thesis, University of Cambridge, Cambridge, UK, 2010.
27. Giardina, G.; DeJong, M.J.; Mair, R.J. Interaction between surface structures and tunnelling in sand: Centrifuge and computational modelling. *Tunn. Undergr. Space Technol.* **2015**, *50*, 465–478. [[CrossRef](#)]
28. Ritter, S.; DeJong, M.J.; Giardina, G.; Mair, R.J. Influence of building characteristics on tunnelling-induced ground movements. *Geotechnique* **2017**, *67*, 926–937. [[CrossRef](#)]

29. Potts, D.M.; Addenbrooke, T.I. A structure's influence on tunnelling-induced ground movements. *Proc. Inst. Civ. Eng. Geotech. Eng.* **1997**, *125*, 109–125. [[CrossRef](#)]
30. Son, M.; Cording, E.J. Estimation of building damage due to excavation-induced ground movements. *J. Geotech. Geoenviron. Eng.* **2005**, *131*, 162–177. [[CrossRef](#)]
31. Franzius, J.N.; Potts, D.M.; Burland, J.B. The response of surface structures to tunnel construction. *Proc. Inst. Civ. Eng. Geotech. Eng.* **2006**, *159*, 3–17. [[CrossRef](#)]
32. Mair, R. Tunnelling and deep excavations: Ground movements and their effects. In *Proceedings of the 15th European Conference on Soil Mechanics and Geotechnical Engineering*; IOS Press: Athens, Greece, 2013.
33. Ritter, S. Tunnel-Soil-Structure Interaction. Ph.D. Thesis, University of Cambridge, Cambridge, UK, 2017.
34. Giardina, G.; DeJong, M.J.; Chalmers, B.; Ormond, B.; Mair, R.J. A comparison of current analytical methods for predicting soil-structure interaction due to tunneling. *Tunn. Undergr. Space Technol.* under review.
35. King, M.; Thomas, I.; Stenning, A. Crossrail project: Machine-driven tunnels on the Elizabeth line, London. *Proc. Inst. Civ. Eng. Civ. Eng.* **2017**, *170*, 31–38. [[CrossRef](#)]
36. Siebenmann, R.; Yu, H.-T.; Bachus, R. UCIMS: Advances in geotechnical construction and performance monitoring. *J. Rock Mech. Geotech. Eng.* **2015**, *7*, 207–212. [[CrossRef](#)]
37. Torp-Petersen, G.E.; Black, M.G. Geotechnical investigation and assessment of potential building damage arising from ground movements: CrossRail. *Proc. Inst. Civ. Eng. Transp.* **2001**, *147*, 107–119. [[CrossRef](#)]
38. Ferretti, A.; Prati, C.; Rocca, F. Nonlinear subsidence rate estimation using permanent scatterers in differential SAR interferometry. *IEEE Trans. Geosci. Remote Sens.* **2000**, *38*, 2202–2212. [[CrossRef](#)]
39. Perissin, D.; Wang, Z.; Wang, T. The SARPROZ InSAR tool for urban subsidence/manmade structure stability monitoring in China. In *Proceedings of the 34th International Symposium on Remote Sensing of Environment*, Sydney, Australia, 10–15 April 2011.
40. Peck, R. Deep excavations and tunneling in soft ground. In *Proceedings of the 7th International Conference on Soil Mechanics and Foundation Engineering*, Mexico City, 1969; Sociedad Mexicana de Mecanica de Suelos: Mexico City, Mexico, 1969; pp. 225–290.
41. O'Reilly, M.P.; New, B.M. Settlement above tunnels in the United Kingdom—Their magnitude and prediction. In *Proceedings of the 3rd International Symposium*; Institution of Mining and Metallurgy: London, UK, 1982; pp. 173–181.
42. Mair, R.J.; Taylor, R.N.; Bracegirdle, A. Subsurface settlement profiles above tunnels in clay. *Geotechnique* **1993**, *43*, 315–320. [[CrossRef](#)]
43. Mair, R.J. General report on settlement effects of bored tunnels. In *International Conference of Geotechnical Aspects on Underground Construction in Soft Ground*; CRC Press: London, UK, 1996; pp. 43–53.
44. Boscardin, M.D.; Cording, E.J. Building response to excavation-induced settlement. *J. Geotech. Eng.* **1989**, *115*, 1–21. [[CrossRef](#)]
45. Timoshenko, S.P. *Strength of Materials: Elementary Theory and Problems*; D. Van Nostrand Company, Inc.: Princeton, NJ, USA, 1957.
46. Vorster, T.; Klar, A.; Soga, K.; Mair, R. Estimating the effects of tunneling on existing pipelines. *J. Geotech. Geoenviron. Eng.* **2005**, *131*, 1399–1410. [[CrossRef](#)]
47. Marshall, A.; Farrell, R.; Klar, A.; Mair, R. Tunnels in sands: The effect of size, depth and volume loss on greenfield displacements. *Geotechnique* **2012**, *62*, 385–399. [[CrossRef](#)]

